Fluid and Impurity Transport during Online Isolation Experiments Conducted with X-Ray Tomography

Sara Ottoboni*[1,2], Muhid Shahid[1,2], Alan Martin[1], Thokozile Kathyola[3], Gunjan Das[3], Sven Schroeder[3], Shashidhara Marathe[4], Christoph Rau[4], Kaz Wanelik[4], Chris John Price, C J[1,2]

[1]EPSRC Centre for Innovative Manufacturing in Continuous Manufacturing and Crystallisation, University of Strathclyde, Glasgow, G1 1RD, UK
[2]Department of Chemical and Process Engineering, University of Strathclyde, Glasgow, G1 1RD, UK
[3]School of Chemical and Process Engineering, University of Leeds, Leeds, LS29JT, UK
[4]Diamond Light Source, Didcot, Oxfordshire, OX11 0DE, UK

Abstract

Pharmaceutical ingredients (API's) need to be pure and have the required particle size distribution, filtration and washing play an important part in achieving this
Fluid flow and impurity transport during filtration, washing a drying are observed using tomography to:

- Visualize the location of impurities during incomplete and complete washing.
- Visualize the consequences of non-ideal filtration and washing
- Visualize residual mother liquor inclusions after washing and link these with agglomeration during drying.

A slurry of API particles, and saturated crystallization solution was filtered to dryland or breakthrough. The effect of particle size distribution was evaluated. Iodine was used to mimic impurities dissolved in the mother liquor and the filter cake was washed with n-heptane. The cake was dried at ambient temperature with flowing gas.
Tomography was used to identify areas where particle agglomeration during drying is favoured.

Key Words: Filtration, washing, drying, fluid and impurity flow, agglomeration, tomography.

1. Introduction

Maintaining particle properties during the downstream isolation is challenging. Breaking or granulation of the crystals may modify the particle size distribution in an uncontrolled way.[1,2] Re-precipitation of dissolved product or of impurities may occur during washing. Any dissolved impurities retained in the cake after washing are incorporated in the product during drying, reducing purity and promoting agglomeration.[3,4, 5]. Isolation was analysed from a macroscopic point of view to understand how particle properties, crystallization and wash solvent properties, impurity characteristics and process procedures affect the final isolated product properties. [6-9]
Typically, at least three cake volumes (5 to 7 ml of solvent per gram of API) of wash solvent is used to remove mother liquor and the associated impurities of synthesis.[7] A deep understanding of; fluid, particles and impurity transport during isolation is needed to improve washing efficiency and improve the environmental isolation sustainability, whilst maintaining product purity,.
Investigation of fluid flows in packed particles beds was previously studied by using synchrotron-based X-ray micro-tomography.[10-16] However, the visualisation of fluid and impurity transport throughout a packed bed of particles during filtration and washing has not been investigated yet. This work uses 2D (time resolved) and 3D tomography as tools to generate this deep understanding of fluid and impurity transport mechanism and microstructure variations during isolation.
Tracking the evolution of the filter cake structure, we will pinpoint the location and migration of impurities during washing as well as the location of residual mother liquor inclusions. Insight into these physical transformations will allow us to design more meaningful procedure to isolate powder beds maximising purity, whilst minimising solvent consumption and particle dissolution or particle agglomeration.
Two different API particle size distribution grades of Paracetamol (PCM) were selected to identify the role of the PSD on microstructure variation and impurity distribution. The crystallisation solvent was ethanol because it is a commonly used solvent to crystallise PCM.[7,17, 18] The wash solvent, n-heptane is miscible with the mother liquors to facilitate both diffusion and dilution washing. Iodine mimics an impurity dissolved

in the mother liquor. It also shows intense X-ray absorption, allowing it to be tracked to evaluate residual mother liquor, to visualise the wash solvent front, and to track impurity locations throughout the cake.
X-ray tomography, in particular, 3D X-Ray Nano-tomography and the 2D time resolved synchrotron X-ray tomography (I13) were used. 3D X-Ray Nano-tomography was used to generate 3D images of the entire cake. These samples were analysed at the end of filtration and washing process to determine microstructure variation and impurity location. The I13 instead was used to study in real time microstructure changes, liquid front profile and location and impurity distribution of isolated samples by collecting time resolved 2D images of a central cake region.
The data collected during the 3D X-Ray Nano-tomography were reconstructed to generate 3D images of the solid cake fraction, where the distribution of larger particles and the particle layering effect were observed (TBTH) and the pore cake fraction where the X-ray absorption indicated the presence of iodine (TBSP). The pore cake fraction 3D structure was used to identify the impurity distribution, and to visualise the wash solvent liquid front (where a drastic reduction of iodine is observed).
The raw data and processed data from the time resolved synchrotron 2D tomography samples, showed fluid and impurity transport during filtration, liquid front evolution and solvent evaporation during filtration, washing, and drying with time resolution of 20 frame per second.

1. Materials and methods

1.1 Materials

Two (grades of Paracetamol granular and micronized) were selected to investigate how particle size distribution affects filter cake microstructure, impurity distribution, and track the liquid front profile. The granular material, x_{50} = 363.58µm, and the micronized material x_{50} = 24.55µm. (Mallinckrodt Inc UK.). Iodine (Merck, UK) was used as an impurity to evaluate wash performance and cake purity by X-ray tomography. Ethanol (Sigma Aldrich, UK), used to create a paracetamol feed suspension. n-heptane (Alfa Aesar, UK) was selected as wash solvent due to the low API solubility 0.0001g/g at 25°C[5]) to investigate displacement and diffusional washing as the crystallisation and wash solvents are miscible.

1.2 Methods

1.2.1 Raw material characterisation

The particle size distribution of micronized and granular material was determined by image analysis (QICPIC, Sympatec, Germany).
The solubility of paracetamol in the crystallization and wash solvents was determined experimentally by equilibration and gravimetric analysis using an incubator on a multi-position stirrer plate.

1.2.2 Suspension preparation

A saturated solution of API in ethanol and a 20%w/V iodine solution in ethanol were prepared. 10µL of the iodine solution was added to 40mL of the API saturated solution to generate the mother liquor solution (ML). 5mL of the ML solution was mixed with 0.8g of paracetamol to make the test slurry.
A series of suspensions of both grades of paracetamol (micronised, **M**, and granular, **G**) allowed the effect of size and size distribution to be assessed.

1.2.3 Isolation experiment X-ray 3D nano-CT experiments

A modified VacMaster (Biotage, Sweden) and a V850 vacuum controller (BÜCHI, UK) were used to filter, wash and then deliquor the paracetamol suspensions using manual best practice. ISOLUTE 6mL double fritted polypropylene reservoirs with 20µm pore size were used to filter, wash and deliquor the cake. The isolation procedure used is reported elsewhere.[5, 9] During the nano-CT experiment the sample is mounted on a rotating stage.
A series of isolation parameters were investigated to understand their effect on microstructure variation, fluid and impurity transport during filtration and washing; paracetamol particle size distribution, (grade), filtration end point (dryland or breakthrough), wash solvent amount (cake volume equivalents), and number of washes. The list of experiments conducted is reported in Table 1.

Table 1 List of 3D X-ray Nano-CT tomography experiments.

Exp	Ethanolic suspension	Filtration	Wash (cake vol)	Exp	Ethanolic suspension	Filtration	Wash (cake vol)
1	PCM, Micronised	Dryland	1 x 2CV	6	PCM, Micronised	Breakthrough	1 x 2CV

2	PCM, Micronised	Breakthrough	1 x 0.5CV	7	PCM, Micronised	Dryland	1 x 3CV
3	PCM, Granular	Breakthrough	1 x 0.5CV	8	PCM, Micronised	Breakthrough	none
4	PCM, Granular	Dryland	1 x 2CV	9	PCM, Granular	Breakthrough	none
5	PCM, Micronised	Breakthrough	1x1.25CV	10	PCM, Micronised	by syringe	none
				11	PCM, Granular	by syringe	none

1.2.4 X-ray 3D Nano-CT experiments and data processing

Samples were analysed in-situ in 6mL Biotage tubes, sealed with parafilm to prevent further solvent evaporation. The sample was exposed to a cone shaped microfocussed X-Ray beam in a Bruker (UK) SkyScan™ 2211 Multiscale X-Ray High-Resolution Nano-tomograph (XRCT) for the time span of image collection at an ambient temperature. The best achievable pixel resolution was 4 µm. Reconstruction of XRCT images was performed utilising Bruker NRecon with the application of the InstaRecon® (CPU) software algorithm. 3D imaging post processing was performed with Bruker CTan software, and 3D rendering and visualization captured using Bruker CTvox and Bruker DataViewer. The reconstructed data was greyscale thresholded to remove both pores, and lightly attenuating material in order to visualise the remaining higher attenuation material indicative of iodine containing cake. Calculations were performed to generate structure separation data, and structure thickness data from this thresholded volume.

1.2.5 Time resolved 2D X-ray synchrotron tomography I13 experiments

Radiographic (2D) phase-contrast images were obtained on beamline I13-2 at Diamond Light Source.[19] A filtered pink X-ray beam was used with a broad-energy of 18 keV – 25 keV, centered at about 23 keV. Carbon (1.3 mm), aluminium (1.4 mm), silver (35 µm) and palladium (42 µm) X-ray filters were used. The Insertion Device (ID) gap and sample-to-detector distance were set to 5 and 10 mm respectively. A Pco.edge 5.5 camera was used in combination with a LuAG 500 µm detector and 2x objective lens (field of view: 6.7 x 5.6 mm; effective pixel size: 2.6 µm); and a CdWO 4500 µm detector and 1.25x objective lens (field of view: 4.2 x 3.5 mm; effective pixel size: 1.6 µm). All 2D images were collected with an exposure time of 0.05 s and acquisition time of 0.05 s. Twenty dark-field and flat-field images were taken in the absence of the X-ray beam and/or sample for background noise correction. Subsequently, projection images of the samples loaded in the filter tube (Figure 1) were collected during the filtration, washing and drying stages. The projection images were processed using bespoke Python scripts, which included flat-field correction (FFC) normalization[20] and image reduction (from 32 to 8-bit depth). The images were then converted into videos using ImageJ.[21]

The setup used for the X-ray time resolved synchrotron tomography experiments is shown in
. The slurry is prepared and transferred to the Biotage 6mL tube that is already in place. To prevent filtrate loss during preparation, the outlet tube was clamped and removed immediately before the beginning of the experiment. The lower peristaltic pump (LP) in Figure 1 was activated remotely and the suspension filtered to form a packed bed of particles either saturated with mother liquor or deliquored. The rotation speed of the peristatic pump controlled the filtration rate. The upper pump (UP) then dispensed wash solvent on top of the cake; reactivating the bottom pump caused the wash solvent to displace the mother liquor. The cake is then deliquored, the residual solvent was mainly the wash solvent with some traces of mother liquor. The cake was then dried at room temperature with air driven using the upper pump. For each step (filtration, washing and drying) the sample is analysed with the I13 beamline.

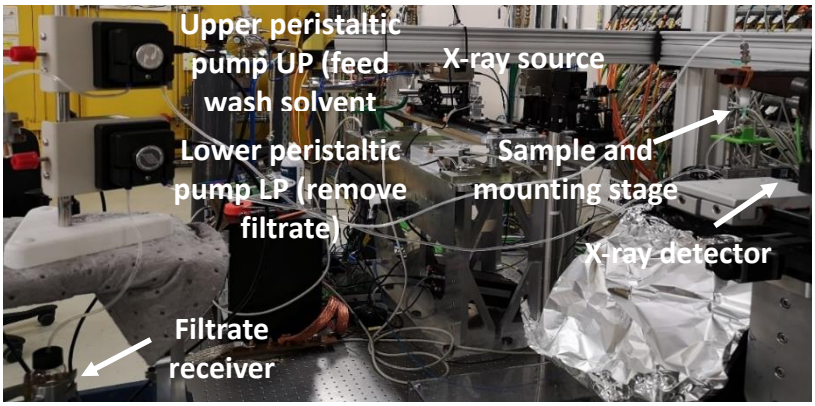

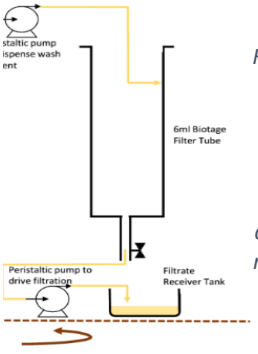

Figure 1 Image of the X-ray 2D time resolved synchrotron tomography and schematic representation of this setup.

The list of experiments conducted and the experimental parameters used is reported in Table 2.

Table 2 List of time resolved 2D X-ray synchrotron tomography experiments.

Exp	Ethanolic suspension	Filtration; Pump flow rate (mL/min)	Wash; Pump flow rate (mL/min)
1	PCM Micronised	Breakthrough; 0.31 UP	1 x 2CV; 0.45 UP & LP
2	PCM Micronised	Dryland; 0.58 UP	1 x 2CV; 0.72 UP 0.45 LP
3	PCM Granular	Dryland; 0.58 UP	1 x 2CV; 0.72 UP 0.45 LP
4	PCM Granular	Dryland; 0.45 UP	1 x 5CV; 0.72 UP 0.45 LP
5	PCM Granular	Breakthroug; 0.45 UP	1 x 5CV; 0.72 UP 0.45 LP

2 Results and discussions

2.1 Cake microstructure variation, fluid transport, and wash solvent profile

The 2D time resolved snapshot images from the reconstructed video (Figure 2) showed the different isolation stages (filtration, washing, and drying). The images in Figure 2 show: (a) ML fluid transport through the porous bed of particles with partial cake deliquoring (b). The transport of impurities is clearly visible with impurity concentration in the bottom part of the cake (Figure 2a, white arrow). The gas feed from the UP may be causing some of the crystallisation solvent to evaporate from the top of the cake (c). The wash front is appearing in (d) which is showing gradual transport of impurities. The filtration step is followed by deliquoring (e), followed by drying where the solvent is evaporated from the cake surface, and then from the cake previously in contact with the walls (f) (due to the cake shrinking occurring during deliquoring).

The wash front profile is generally clearer to observe in cake formed by micronized particles because of its larger surface area and more uniform pore size distribution. Comparing experiment 1 (Figure 3, left) and Figure 3 (right), micronized cake shows a clear wash front with a curved profile, while the granular cake, for its large porosity and broad pore size distribution, facilitate the wash solvent permeability and removal.

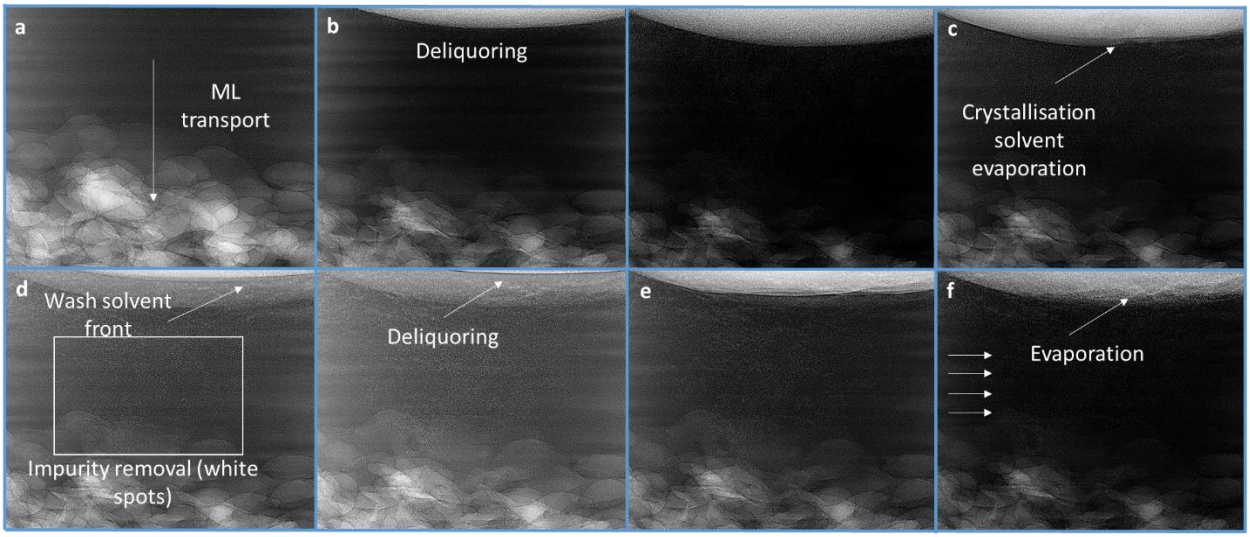

Figure 2 Snapshot of time resolved 2D X-ray synchrotron tomography experiment 3.

The effect of the particles size (grade) on purity is seen comparing experiment 1 with experiment 4, Figure 3.

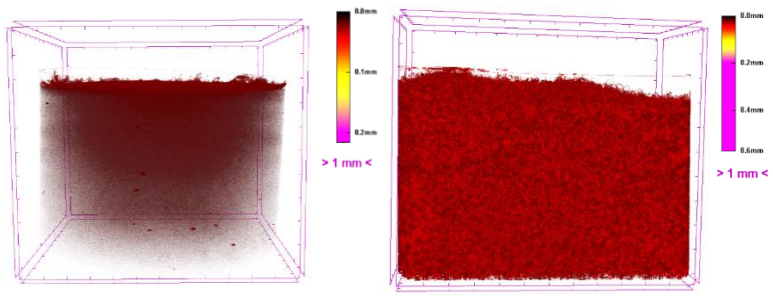

Figure 3 Pore fraction 3D images of experiment 1 (left) and experiment 4 (right).

2.2 Filtration halting point effect and iodine distribution

Analysing the binarized images of experiment 1, 2, and 6 the effect of filtration halting method (dryland or breakthrough) was observed. The effect of maintaining saturated cake with mother liquor before dispensing the wash solvent showed no cake surface disturbance (experiment 1, Figure 4, left), while longitudinal cake damages, similar to an "exfoliation effect", (experiment 6, Figure 4, centre) or cake shrinking from the filter walls (experiment 2, Figure 4, right) could be observed in case of filtration stopped at breakthrough. In case of filtration stopped at dryland, a more even distributed and rounded washing front is observed (red), while for experiments where the filtration was halted at breakthrough the washing front is less uniform and characterised by impure areas trapped between longitudinal voids where the impure mother liquor was removed (see Figure 4 centre). The rounded wash profile can resemble to the porosity anisotropic profile observed in the cake cross-section:[22, 23] near the walls there is high probability of loose packing due to the different material interaction (particle-wall) with consequence increase of porosity. Instead, the core of the cake is generally more tightly packed, forming a uniform microstructure.

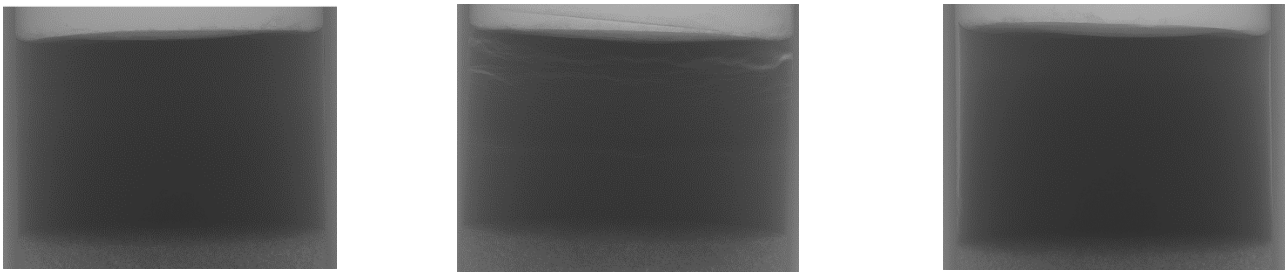

Figure 4 Binarized images of experiment 1 (left), 2 (right), and 6 (centre).

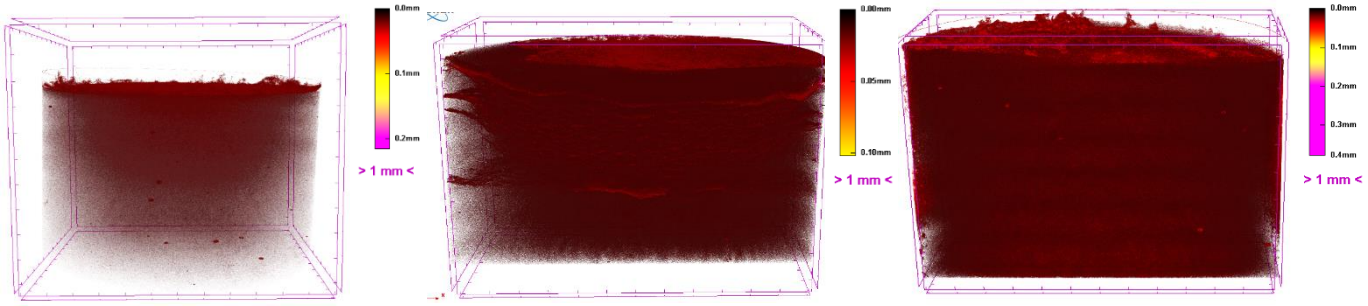

Figure 5 Pore fraction 3D images of experiment 1 (left), experiment 6 (centre), and experiment 2 (right).

These kind of damages are then responsible of ineffective washing (Figure 4). Even if the cakes of experiment 2 and 6 seems purer than the cake of experiment 1, the impure areas trapped in cake filtered to
These kind of damages are then responsible of ineffective washing (Figure 5). Even if the cakes of experiment 2 and 6 seems purer than the cake of experiment 1, the impure areas trapped in cake filtered to breakthrough are less accessible for the wash solvent because those areas are surrounded by voids (longitudinal cracks) that operates as preferential wash solvent path.

2.3 Amount of wash solvent used

To describe the effect of the volume of wash solvent used during a single wash, the pore fraction 3D images of experiment 5, 6 and 8 were used (Figure 6).

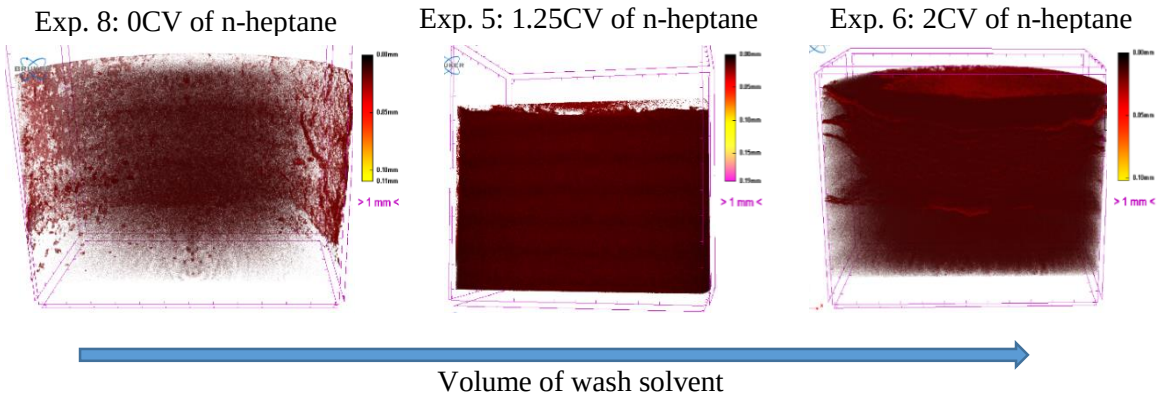

Figure 6 Pore fraction 3D images of experiment 8 (left), experiment 5 (centre), and experiment 6 (right).

In case the cake was not washed (experiment 8), the iodine content is much higher respect the cakes where a washing step was operated (experiment 5 and 6). In detail, the iodine is more concentrated (white area) around the walls with a decrease in iodine gradient content from walls to the bulk. This effect can be correlated to the wall effect. The red layer around the walls is resembled to the shrinking cake effect caused by the breakthrough filtration stopping procedure (visible from the binarized image). Future plan is to use chromatographic technique to quantify the mean residual iodine concentration. Increasing the amount of wash solvent used improves the impurity removal efficiency.

3 Conclusions

X-ray tomography (Nano-CT) has been shown to track impurities during filtration and washing. It can identify disruption and variation after filtration and washing, and could visualize the wash front. However, the data accumulation time used with this technique was sufficiently long to prevent real time on-line measurement. Another limitation of the Nano-CT is the relatively low contrast between iodine rich and depleted regions which limits accurate location of impurities. Using the time resolved 2D synchrotron X-ray tomography (I13) it will be possible to analyse in real-time the microstructure variation occurring during filtration (cake compaction due to the filtrate removal) and the fluid and impurity transport through the cake.

4 References

(1) Lekhal, A., et *al*., 2003. Powder Technol. 119. **(2)** Lekhal, A., et *al*., 2004. Int. J. Pharm., 263. **(3)** Ruslim, F., Hoffner, B., et *al*.., 2009. Chem. Eng. Res. Des., 1075. **(4)** Kuo, M., T., Barrett, E., C., 1970. AIChE J., 633. **(5)** Ottoboni, S. Ph.D. thesis. Dept. of Chemical and Process Engineering, University of Strathclyde, Glasgow, UK, 2018. **(6)** Ripperger, S., Gösele, W., et *al*., Major Reference Works, 2013. **(7)** Murugesan S., et *al*., Wiley New York, 2010. **(8)** Beckmann, W. Wiley-VCH, 2013. **(9)** Ottoboni, S., Price, C., et *al*., 2018. Journal of Pharmaceutical Science, 1. **(10)** Berg, S., et *al*., 2013. PNAS, 3755. **(11)** Culligan, K., A., et *al*., 2006. Advances in Water Resources, 227. **(12)** Charvet, A., et *al*., 2011. Chemical Engineering Science, 624. **(13)** Al-Raoush, R., et *al*., 2005. Journal of Hydrology, 44. **(14)** Al-Raoush, R., et *al*., 2005. Journal of Hydrology, 44. **(15)** Bierck, B., R., et *al*., 1988. Water Environment Federation, 645. **(16)** Arora, S., Dhaliwal, S., et *al*., 2006. Computer and Chemical Engineering, 1054. **(17)** Thompson, C.; Davies, M., C., et *al*., 2004. Int. J. Pharm.., 137. **(18)** Ellis, F. Royal Society of Chemistry, 2002. **(19)** Rau, C., 2017. Synchrotron Radiation News, 19. **(20)** Van Nieuwenhove, V., De Beenhouwer, J., et *al*., 2015. Optics Express, 27975. **(21)** Schneider, C., A., Rasband, W., S., et *al*., 2012. Nature Methods, 671. **(22)** Fathi-Najafi, M., Theliander, H., 1995. Sep. Technol., Progress in Separations and Waste Reduction, 165. **(23)** Tiller, F., M., Haynes, S., et *al*., 1972. AIChE J., 13.